Proceedings of ISERME 2025
19-20 September 2025
https://doi.org/10.31705/ISERME.2025.21

Modified Kaolinite Fine Clay to Remove Lead from the Contaminated Water

Thepulasingha[1] TMKC, Weerasinghe[1] WMLB, Tepeeskan[1] L, Fernando[2] WAM and Wickrama[1] MADMG

[1]Department of Earth Resources Engineering, University of Moratuwa, Sri Lanka

[2]Department of Nanoscience Technology, Wayamba University, Sri Lanka

*Corresponding author - maheshwari@uom.lk

Abstract
Kaolinite clay has emerged as a valuable material in environmental remediation, particularly for treating contaminated water. This study examines the potential of kaolin clay, in both its raw and modified forms, for the efficient removal of heavy metals, particularly lead (Pb), from wastewater. The unique physical and chemical properties of kaolin, such as its high surface area, adsorption capacity, and structural stability, make it an effective adsorbent for a wide range of contaminants. This research evaluates various modification methods, including acid activation, intercalation, and calcination. Treatment with coal fly ash, aimed at enhancing its adsorption properties through intercalation, is also investigated. Characterization techniques such as X-ray Diffraction (XRD), Scanning Electron Microscopy (SEM), and Fourier Transform Infrared Spectroscopy (FTIR) were employed to assess the structural and chemical changes induced by these modifications. Adsorption kinetics were evaluated to measure effectiveness during the study. The study showed higher lead adsorption in coal fly ash-treated kaolin compared to its raw form. Kaolin clay, being a naturally abundant and cost-effective mineral, presents a sustainable solution for water treatment, demonstrating significant potential for future applications in heavy metal removal.

Keywords: Adsorption, Heavy metal removal, Lead (Pb), Modified Kaolin clay, Water treatment

1 Introduction

According to the UN SDG Report (2023), access to clean and safe drinking water remains a global challenge. As mentioned by Mukhopadhyay [1], rapid industrialization, intensive agricultural practices, and various harmful anthropogenic activities—such as pollution from industrial waste, deforestation, improper waste disposal, and mining—are the main causes of this critical global issue. Among these contaminants, Pb (lead) is one of the most hazardous heavy metals frequently found in polluted water sources, and even at low concentrations, it poses severe risks to human health [2]. Because of this, effective Pb removal has become a key component of modern water purification systems. With limited naturally occurring safe water reserves, the world is now largely dependent on engineered purification methods to fulfill potable water requirements. However, due to their high operational and capital costs, many developing countries have low adoption of advanced techniques such as reverse osmosis, ion exchange, electrolysis, and electrodialysis. Therefore, adsorption-based methods are widely favored because of their cost-effectiveness, efficiency, and environmental sustainability [3].

In this context, fine clay is one of the naturally abundant adsorbent materials, known for its high surface area and modifiable properties [4]. The objective of this study is to investigate the adsorption efficiency of natural and modified fine kaolinite clay for Pb removal, focusing on structural characterization and the adsorption isotherm. Intercalation with industrial ashes, calcination, and acid treatments were selected as modification processes to enhance Pb adsorption performance while maintaining low cost and material sustainability.

To further support this objective, adsorption kinetics were examined, as kinetic studies describe the rate at which an adsorbate is removed from a solution and transferred onto the

surface of an adsorbent. Designing an effective adsorption system requires a better understanding of adsorption kinetics. By analyzing the kinetic behaviour, observers can gain insight into the adsorption mechanism and identify the rate-controlling steps involved in the adsorption process [5]

2 Methodology

2.1 Materials

The fine kaolin clay sample (WC 8560) was obtained from Lanka Mineral and Chemicals (PVT) Ltd. It is a purified natural clay mined from quartz deposits in the Matale District, with an average particle size of less than 7.5 μm. The coal fly ash (CFA) was collected from the Lakvijaya Coal Power Plant using a convenience sampling method by the authors of the study [6]. All other chemicals used were of analytical reagent grade, and the standard Pb AAS solution had a concentration of 1000 ppm

2.2 Clay Modification

Using a Raw Kaolin(RW-K) clay sample, 2 types of modified clay samples were obtained.

a. Calcinated and Acid-activated (CA-K)
b. Treated by Coal Fly Ash (CFA-K)

Clay modification process 1**:** Calcined and acid-activated Kaolin

Approximately 50 g of raw kaolin clay was subjected to calcination in a muffle furnace (Gallenkamp, Weiss Technik UK Ltd.) at 850 °C for 3 hours. The temperature profile achieved during the process is presented in Table 1. The calcined samples were then allowed to cool gradually to room temperature in a desiccator before being used for acid activation.

Table 1- Temperature variation with Time during calcination

Time	**1h**	**2h**	**3h**
Temperature	570^0C	800^0C	850^0C

The calcined kaolin (15 g) was then treated with a 1:1:1 (v/v) mixture of concentrated HNO_3 (50 mL, 69–72%), H_2SO_4 (50 mL, 95–97%), and H_3PO_4 (50 mL, 88%) under constant stirring (450 rpm) at 50 °C for 2 hours. After cooling to ambient temperature, the slurry was filtered through a 1 μm membrane, followed by repeated washing with deionized water until a neutral pH was achieved. Due to low solid recovery, the final product was dried at pH 2 and stored in airtight containers for subsequent characterization.

Clay modification process 2: Kaolin treated by ash Extract

Forty grams (40 g) of fly ash was homogenized with 400 mL of deionized water (1:10 w/v ratio) under continuous magnetic stirring (450 rpm). To enhance the solubility of silica and alumina species, 8 g of sodium hydroxide (NaOH, 0.5 M analytical grade, >99%) was added to the suspension. The mixture was maintained at an ambient temperature (25±1°C) for 2 hours, followed by filtration through a 1 μm filter paper. The resultant alkaline extract was stored until further use.

Subsequently, twenty grams (20g) of raw kaolin was reacted with 200 mL of the above ash extract (1:10 solid: liquid). The system was heated to 85±0.5°C with constant mechanical stirring (400 rpm) for 2 hours to facilitate ion exchange. The suspension was then aged for 24 hours at room temperature to promote structural reorganization. The modified clay was recovered through filtration, rinsed with deionized water until a neutral pH was attained, and dried at 105°C for 24 hours.

Finally, the dried product was mechanically homogenized using a lab-scale Tema mill to ensure uniform particle size distribution.

2.3 Characterization of kaolin

The infrared spectroscopy of all modified and raw clay samples was obtained using a Fourier transform infrared (FT-IR) spectrometer (KBr,400-4000cm^{-1}). The Crystallinity of the five samples was determined by powder X-ray diffraction (Ultima IV) with Cu-Kα radiation (λ = 1.5418Å) operated at 40kV and 30mA. The XRD pattern was recorded from 0^0 to 80^0 of 2θ with a step size of 0.01^0. Solid Morphology and average particle size were analyzed by scanning electron microscopy (SEM) under 10kV.

2.4 Kinetics of Pb adsorption

A stock solution of 100mg/L(100ppm) of Pb solution was prepared from a 1000mg/L Pb AAS standardized solution. The kinetics of Pb adsorption were studied at 45℃, with contact times ranging from 0 – 4 minutes. The adsorbent amount of 2 g was used with 50 mL from the previously prepared stock solution. All modified and raw samples were tested under these

conditions. The following formula was used to calculate the amount of lead ions adsorbed by the adsorbent:

$$\mathbf{Q_t\left(\frac{mg}{g}\right) = \frac{(C_0\text{-}C_t).V/1000}{W}} \qquad \mathbf{(1)}$$

Where Q_t is the amount of metal ions adsorbed on the adsorbent at time t, C_0 is the initial metal ion concentration (mg/L), C_t, the concentration of metal ions at time t (mg/L), V, the volume of the metal ions solution used(mL), and W is the weight of the adsorbent used (g).

2.5 Adsorption Kinetics

Y.S.Ho developed a pseudo-second-order kinetic expression for the adsorption system, and equations 2 and 3 are one of the widely applied model for many metal sorption systems[7]. Linear form:

$$\frac{t}{Q_t} = \frac{1}{kQ_e^2} + \frac{t}{Q_e} \qquad (2)$$

Where $Q_e$is the amount of Pb adsorbed at equilibrium (mg/g), Q_t is the amount of Pb adsorbed at time t (mg/g) and k is the rate constant of the pseudo-second-order model. The initial adsorption rate h was obtained according to the equation below:

$$\mathbf{h = kQ_e^2} \qquad \mathbf{(3)}$$

An adsorption process best fitting with the pseudo-second-order model indicates that the chemically dominant system[5].

2.6 Data analysis

Python programming was used to analyze the XRD dataset. Custom scripts were written to preprocess and visualize the data using the Pandas, NumPy, and Matplotlib libraries. Peak detection was performed with a threshold of 1000 cps, a minimum prominence of 5 cps, and a minimum peak-to-peak distance of 0.250° 2θ. Subsequently, the d-spacing values were calculated using Bragg's Law.:

$$\mathbf{n\lambda = 2dsin\theta} \qquad \mathbf{(4)}$$

Where λ is the wavelength of the radiation and d is the basal interlayer space. (n is an integer), θ is the angle of the incidence.

To analyze SEM images, ImageJ software was used. To count the particles, total particle area, and average particle sizes Intermodes threshold algorithm was used with the watershed tool. For all samples defined the minimum particle size and total image cover area were 0.1 nm^2 and 230 nm^2. Then FTIR results were analyzed manually, comparing the raw kaolin pattern.

3 Results and discussion

3.1 Characterization of Kaolin

The FTIR spectrum reveals significant structural changes in kaolin after treatments. In the CA-K clay, the O–H stretching bands at 3695–3697 cm^{-1}, 3622–3623 cm^{-1}, and 3432–3424 cm^{-1} [7] disappear (Figure) indicating the complete dihydroxylation of kaolin. The Al–OH bending peak at 1451–1446 cm^{-1} also vanishes, confirming structural breakdown of the alumina layers. Additionally, a new C–H stretching band appears at 2926–2925 cm^{-1} [8], suggesting the presence of organic residues.

In the ash-treated sample (CFA-K), some O-H bonds are retained(Figure), while new peaks emerge at 482$cm^{-1}$and 490cm^{-1} (Si-Si vibration) [9] and 435–419 cm^{-1} (Metal–O stretching) [10], indicating silica enrichment and metal incorporation.

RW-K exhibited a particle count of 180, with a total particle area of 85.013nm^2. The calculated average particle size was 0.0472nm with surface coverage of 36.459%. The modification treatments resulted in significant morphological changes, as summarized in Table 2. The CA-K, CFA-K samples showed an increase in both total particle area and average particle size, suggesting that particle growth or agglomeration due to the modification, as illustrated in Figures 3,4, and 5.

The characteristic peaks corresponding to the (001), (002), and (004) planes were identified based on standard diffraction data for kaolinite clay. The typically basal reflection(001) observed at 2θ=12.3^0 [10] in kaolinite, was most prominent in the unmodified clay sample (RW-K). In this study, the (001) peak was clearly visible only in the RW-K sample (Table 3), which suggests that the unmodified sample has preserved its crystallinity. The modified CFA-K sample showed the absence of the (001) reflection, indicating disruption or exfoliation of the basal layer, indicating the unmodified sample retained its crystallinity. In contrast, the modified CFA-K sample showed the absence of (001) reflection,

Additional peaks at 2θ = 24.8^0 and 50^0, which correspond to the (002) and (004) planes[10] were observed in both modified samples. A

strong, sharp peak around $2\theta = 27.5^0$ was observed in the samples, which corresponded to the Quartz (SiO_2).

3.2 Adsorption Kinetics

The kinetics of four modified samples and unmodified samples were analysed using the Pseudo-second order model, and each data set showed the best fit (Figure 6). The equilibrium adsorption capacities (Q_e) varied significantly among the samples (Table). CFA-K exhibited the highest capacity at 1.819mg/g, while CA-K showed lower capacities than the RW-K (0.987mg/g). This may be attributed to a higher pH value. The kinetic rate constants(k) also differed. Fastest rate constants show the CA-K at 10.471 g/mg.min respectively. CFA-K showed lower rate constants than the RW-K rate (4.2422g/mg.min). Results indicated that CFA-K modification significantly enhances the adsorption capacity. Figure 7 shows the variation in supernatant lead concentration over time with different adsorbents.

Table 2-SEM analysis results table

Property	RW-K	CA-K	CFA-K
Particle Count	180	170	252
Total Particle Area(nm^2)	85.013	184.608	107.613
Average Particle Size (nm)	0.472	1.086	0.472
%Area	36.459	79.171	46.241

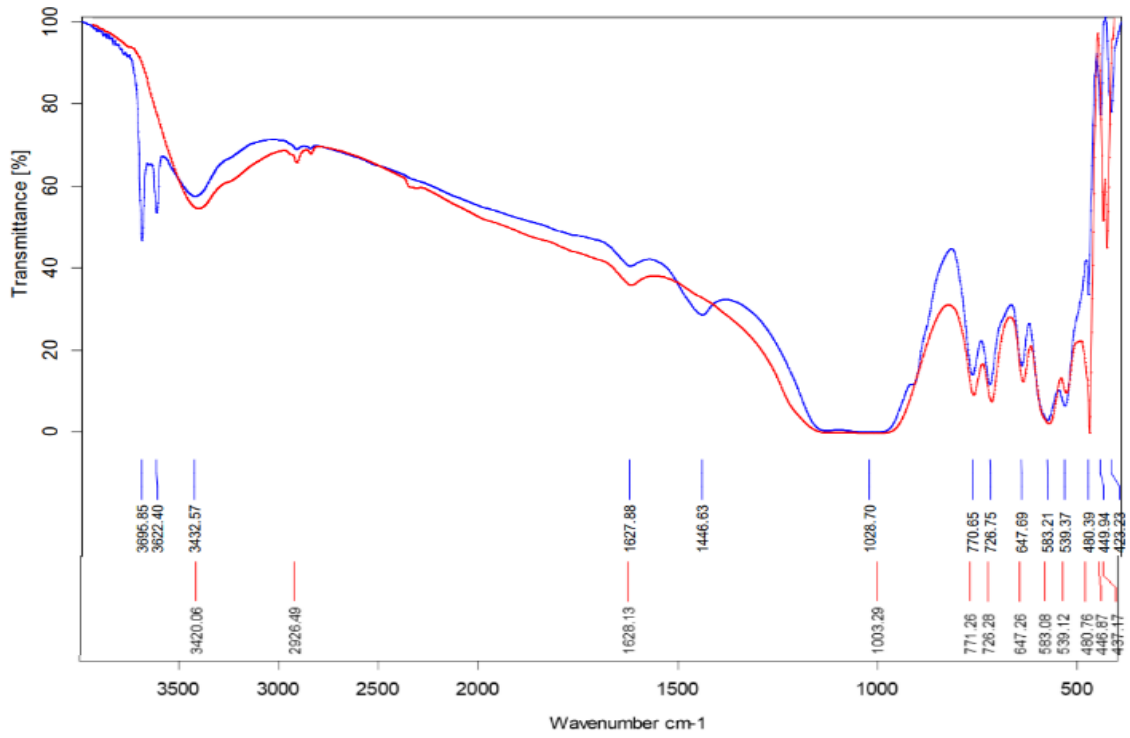

Figure 1 - FTIR curves of RW-K(Blue) vs CA-K

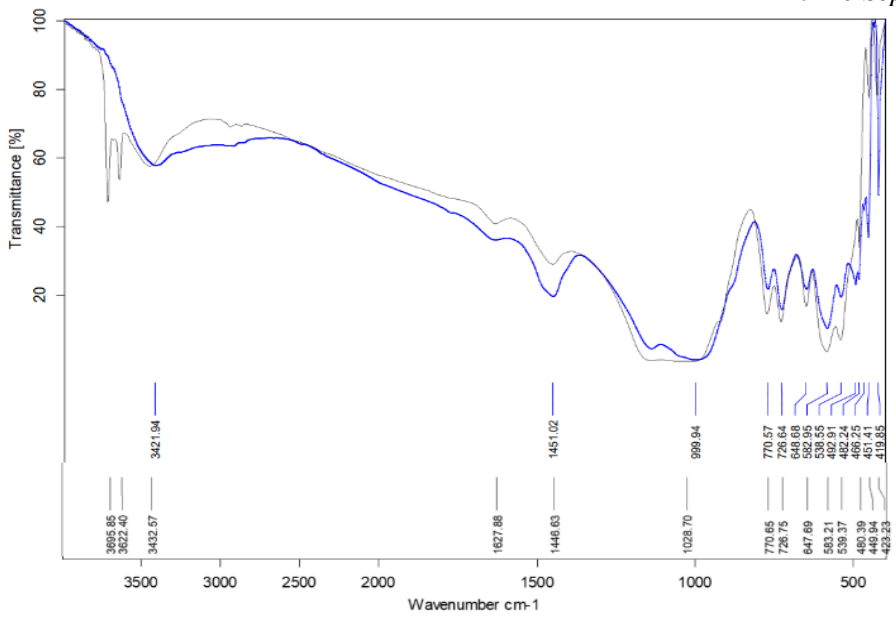

Figure 2 - FTIR curves of RW-K vs CFA-K(Blue)

Table 3 – Corresponding 2θ values for identified peaks for each sample

RW-K	CA-K	CFA-K
12.341	13.714	13.733
13.712	21.113	14.066
21.097	22.498	21.111
22.463	23.241	22.433
23.242	23.492	23.322
23.572	23.82	23.597
23.934	24.096	24.081
24.187	24.473	24.427
24.454	24.774	24.734
24.955	25.679	25.694
25.709	26.44	26.432
26.514	26.695	26.695
26.784	27.157	27.127
27.171	27.524	27.554
27.585	29.662	29.504
27.861	29.922	29.821
29.58	30.253	30.272
29.851	30.881	30.851
30.248	32.405	32.379
30.676	34.506	34.415
30.942	35.009	34.767
32.454	35.273	35.259
34.359	35.535	41.873
34.709	41.848	42.852
35.003	42.914	50.593
35.4	47.251	50.885
35.661	50.645	-
41.898	50.906	-
47.225	-	-
50.668	-	-
50.941	-	-

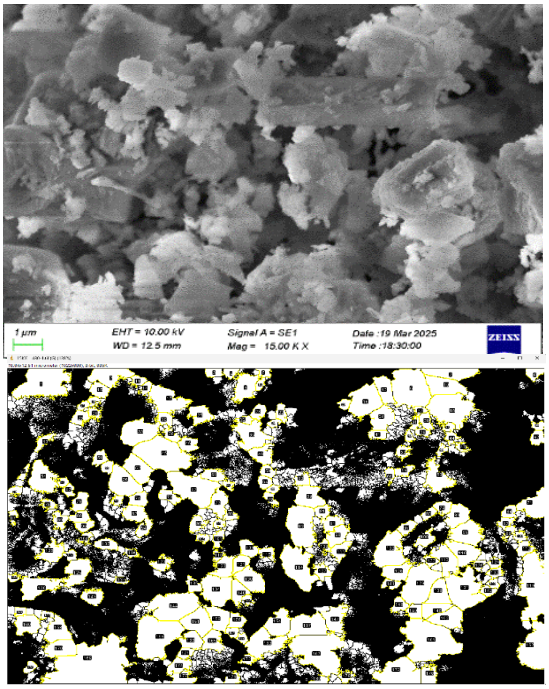

Figure 3 - RW-K SEM image(upper), and corresponding binary image generated by Intermodes algorithm

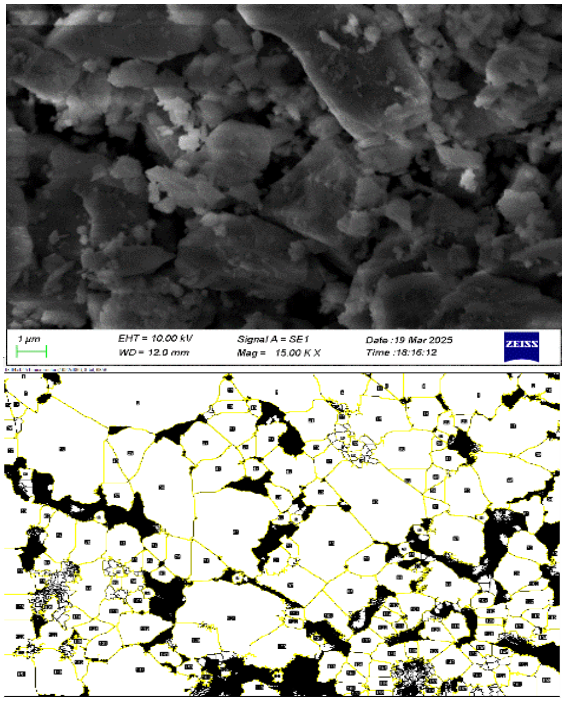

Figure 4 - CA-K SEM image(upper), and corresponding binary image generated by Intermodes algorithm

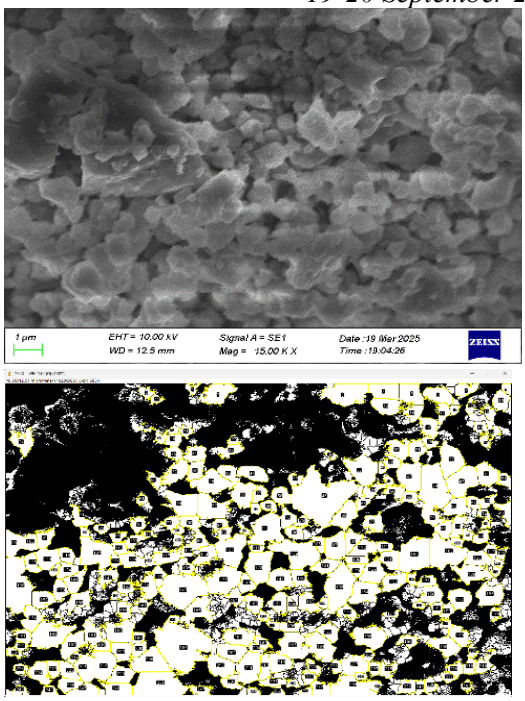

Figure 5 - CFA-K SEM image(upper), and corresponding binary image generated by Intermodes algorithm

Table 4-Pseudo-Second-Order rate constant and measured parameters for different clay types

Clay Type	R^2	Q_e(mg/g)	k(g/mg.min)	h(mg/(g.min))
RW-K	0.9985	0.9873	4.2422	4.1356
CA-K	0.9943	0.5884	10.471	3.6258
CFA-K	0.9919	1.8192	2.1294	7.0472

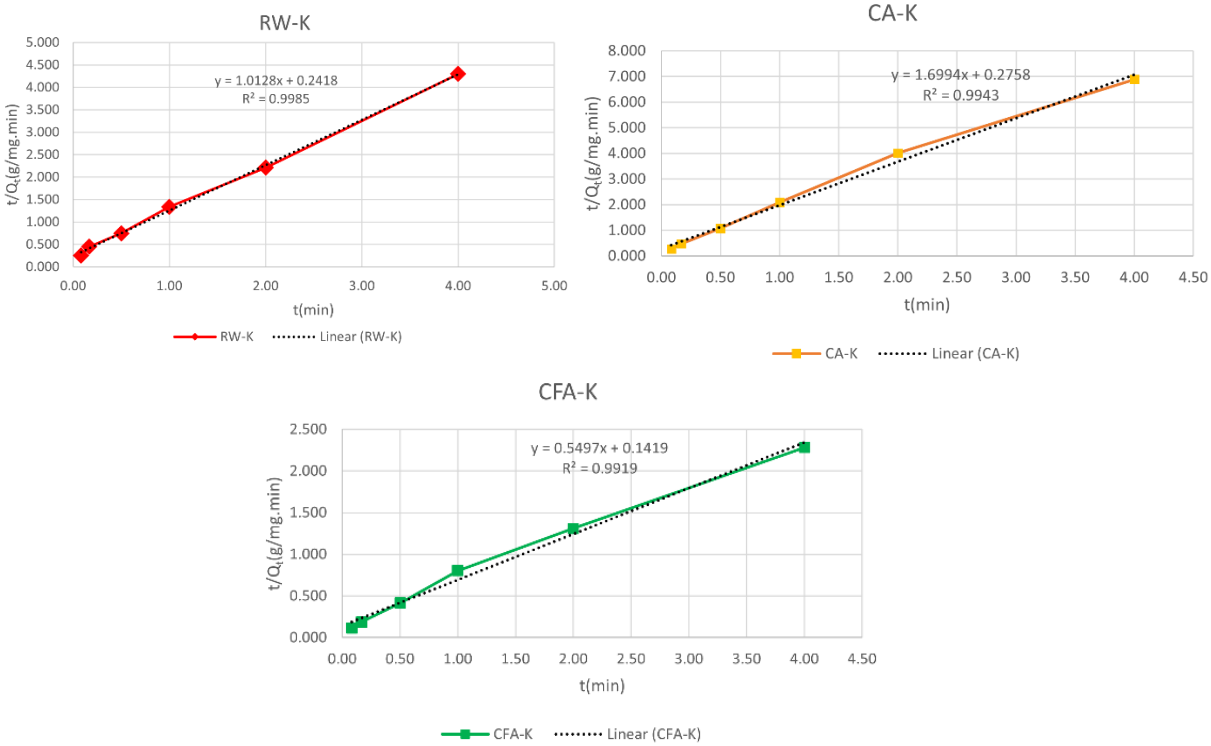

Figure 6 - Pseudo-second-order graphs for RW-K, CA-K, and CFA-K

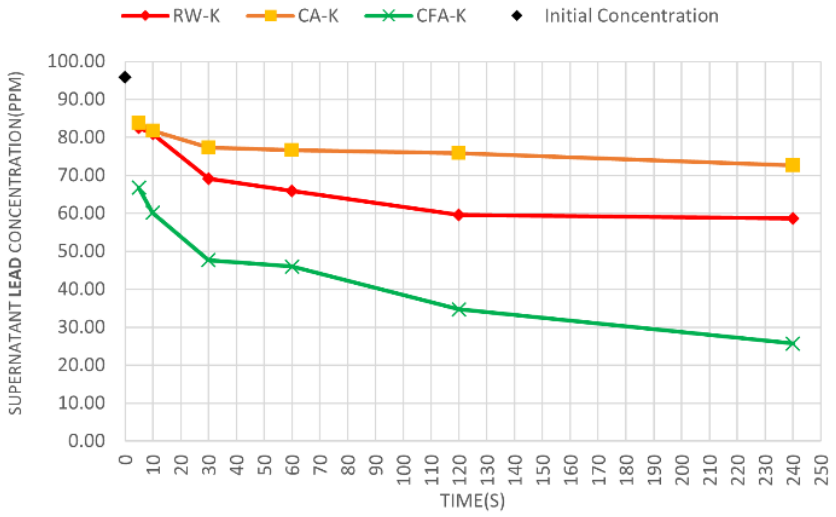

Figure 7 - Supernatant lead Concentration variation with time

4 Conclusion

Both modification methods resulted in structural and morphological changes within the Kaolinite structure.

Adsorption Kinetics analysis emphasizes that kaolin treated by coal fly ash is the most promising candidate for lead removal from wastewater among other adsorbents.

The linearity of pseudo-second-order plots indicated that chemisorption is the dominant system rather than physisorption.

Furthermore, the combination of the modification process and intercalation with ashes demonstrated enhanced adsorption performance, suggesting a synergistic effect.

Acknowledgements

The authors convey their heartfelt gratitude to the Department of Earth Resources Engineering, the Department of Civil Engineering, and the Department of Materials Science and Engineering at the University of Moratuwa for their invaluable academic guidance and continued support throughout the study. Furthermore, the authors sincerely appreciate the assistance extended by the laboratory staff of the above departments for facilitating the required analyses, including FTIR and SEM testing. Special thanks are extended to Dr. Upeka Samarakoon of the Department of Nanoscience Technology, Wayamba University of Sri Lanka, for conducting the XRD analysis and providing expert insights into the interpretation of the results. Finally, the authors gratefully acknowledge the managing team of Lanka Minerals and Chemicals (Pvt) Ltd. for their generous support and provision of essential resources that significantly contributed to the successful completion of this research.

References

[1] R. Mukhopadhyay *et al.*, 'Clay–polymer nanocomposites: Progress and challenges for use in sustainable water treatment', *Journal of Hazardous Materials*, vol. 383, p. 121125, Feb. 2020, doi: 10.1016/j.jhazmat.2019.121125.

[2] Shakoor, H., Alshehri, F., Shahab, M., Abanumay, F. A., & Ali, L. (2025). Vulnerability and risk assessment of lead (Pb) concentrations in drinking water via statistical and geostatistical analyses. Frontiers in Water, 7.doi.org/10.3389/frwa.2025.1548110

[3] E. I. Unuabonah and A. Taubert, 'Clay–polymer nanocomposites (CPNs): Adsorbents of the future for water treatment', *Applied Clay Science*, vol. 99, pp. 83–92, Sep. 2014, doi: 10.1016/j.clay.2014.06.016.

[4] A. Amari, F. Mohammed Alzahrani, K. Mohammedsaleh Katubi, N. Salem Alsaiari, M. A. Tahoon, and F. Ben Rebah, 'Clay-Polymer Nanocomposites: Preparations and Utilization for Pollutants Removal', *Materials*, vol. 14, no. 6, p. 1365, Mar. 2021, doi: 10.3390/ma14061365.

[5] H. Mosaddeghi, H. Masoudi, and fatemeh ravari, 'Removal of Nitrate from Water by Modified Nano Clay and Comparison with Nano Graphene, Nano Fe3O4 and Nano

Clay – Isotherm and Kinetics study', *Desalination and water treatment*, Jul. 2019, doi: 10.5004/dwt.2019.24644.

[6] V Amirthavarman *et al.*, 'Experimental synthesis of zeolites from pre-processed coal fly ash using the microwave irradiation method', in *Proceedings of International Symposium on Earth Resources Management and Environment*, Division of Sustainable Resources Engineering, Hokkaido University, Japan, 2024, pp. 170–178. doi: 10.31705/iserme.2024.27.

[7] M. Jiang, Q. Wang, X. Jin, and Z. Chen, 'Removal of Pb(II) from aqueous solution using modified and unmodified kaolinite clay', *Journal of Hazardous Materials*, vol. 170, no. 1, pp. 332–339, Oct. 2009, doi: 10.1016/j.jhazmat.2009.04.092.

[8] J. Coates, 'Interpretation of Infrared Spectra, A Practical Approach', in Encyclopedia of Analytical Chemistry. , John Wiley & Sons Ltd, 2006, pp. 10815–10837.

[9] N. Ahmed, C. B. Singh, S. Bhattacharya, S. Dhara, and P. B. Bhargav, 'Raman and FTIR Studies on PECVD Grown Ammonia-Free Amorphous Silicon Nitride Thin Films for Solar Cell Applications', *Conference Papers in Energy*, vol. 2013, pp. 1–4, May 2013, doi: 10.1155/2013/837676.

[10] K. Nakamoto, *Infrared and Raman Spectra of Inorganic and Coordination Compounds: Applications in Coordination, Organometallic, and Bioinorganic Chemistry*, 6th ed. Newy York: John Wiley & Sons, Incorporated, 2009.

[11] R. Dewi, H. Agusnar, Z. Alfian, and Tamrin, 'Characterization of technical kaolin using XRF, SEM, XRD, FTIR and its potentials as industrial raw materials', *J. Phys.: Conf. Ser.*, vol. 1116, p. 042010, Dec. 2018, doi: 10.1088/1742-6596/1116/4/042010.